3

Background guided parabolic pulses in dispersion decreasing fiber for long distance stable pulse delivery

3.1 Introduction

The demand of high power ultrashort pulse delivery has been exponentially growing with the rapid advancement in the field of science and technology, as well as in every civil and strategic purposes that employ the advanced technology for their own development. Lately, there is a huge requirement of high power light sources in a diverse fields of application such as - the chemical industry for various remote spectroscopic measurements [Bračun and Selak, 2018]; the bio-medical industry for optics based diagnosis and surgery [Lee et al., 2013]; in laboratory-based complex scientific experiments; and for the exclusive purpose of strategic applications [Curtis et al., 2014]. Such wide range of applications eventually demand compact, robust and easy-to-implement systems/devices that will deliver stable and self-consistent high power optical pulses. For this, optical fiber based systems possess huge potential due to their strong light guiding mechanism, structural compactness and flexibility, as well as integration feasibility with the existing network. However, it has already been discussed in chapter 1 that such high power ultrashort pulses undergo wave-breaking due to the onset of gradually growing nonlinear interactions during their propagation through the fibers that eventually limits their utilities. As a remedy to combat OWB, a special parabolic pulse form with linear frequency chirp has been proposed which is known to be robust against strong nonlinearities [Anderson et al., 1993]. Such parabolic pulses can be generated in fibers via pulse reshaping technique owing to the counterbalanced action of normal dispersion, nonlinearity and distributed gain/loss. Notably, the presence of gain in fiber amplifiers have been very suitable for the generation of parabolic pulses. However, the amplifiers pose certain challenges like limited amplifier bandwidth, and noise amplification that put restrictions on the parabolic pulse forms; sometimes leads to their distortion. Eventually, the need of passive medium based pulse reshaping i.e., without amplification, becomes important to obtain pure parabolic pulses. It is possible to achieve parabolic pulses in passive fibers via decreasing dispersion profile [Hirooka and Nakazawa, 2004]. It has been observed that the decreasing dispersion induces a length dependent factor Γ that plays the role of the constant amplifier gain. Furthermore, such passive medium based reshaping can be done in two regimes - one is nonlinearity dominated reshaping, and the other is dispersion dominated reshaping [Sukhoivanov et al., 2013]. The dispersion dominated reshaping is a comparatively slower pulse reshaping process in which the dispersion length L_D and the nonlinear length L_{NL} are comparable, i.e., in case of fibers with lower nonlinearities (such as silica based fibers). Moreover, this regime of operation necessarily need not to have a decreasing dispersion profile, and can be achieved in a normally-dispersive straight fiber too. On the other hand, the nonlinearity dominated reshaping occurs mainly in presence of decreasing dispersion along with a large fiber nonlinearity such that $L_D >> L_{NL}$. In that case, the parabolic pulses are formed much

faster within a short length of the fiber and with further accumulation of nonlinear phases, the frequency chirp starts to become non-monotonous leading to OWB. This regime of reshaping is often referred to as *intermediate transient state*. Thus, it is necessary for highly nonlinear fibers to overcome the intermediate state of reshaping for stable propagation of parabolic pulses over long distances. For the first level of investigation towards this aim, customization of the initial optical pulse has been opted as a solution to achieve stable high power ultrashort pulse delivery.

In this chapter, a detailed and systematic investigation on possible stable delivery of high power ultrashort pulses through a kilometer long fiber has been presented to meet the existing technological challenges. The asymptotic evolution and stable propagation of parabolic pulses from a background-guided input seed pulse has been extensively studied. Since, the asymptotic evolution is largely dependent on input pulse energy, here we establish that presence of a background dark pulse will eventually stabilize its propagation over longer distances. In the first section, the design of a dispersion decreasing Bragg fiber (DDBF) has been discussed to operate at 0.98 μm wavelength. Moreover, the formation of parabolic pulses in such DDBF has also been presented. In the subsequent section, pulse reshaping through a several-kilometer long DDBF has been studied by feeding the fiber with a Gaussian seed pulse and a hyperbolic-secant (sech) pulse both guided by a hyperbolic-tangent (tanh) pulse of a very small width. Moreover, a comparative study has been presented between the propagation of the background guided-pulses with that of the unguided pulses through the same DDBF to establish the significance of the adapted technique.

3.2 Dispersion decreasing fiber

Fiber tapering is the technical process to achieve a decreasing dispersion profile. It involves heating and simultaneous slow pulling of the straight fiber which eventually changes the dimensions of the fiber cross-section over the length, and eventually affects the optical performance of the fiber [Xue et al., 2007]. The dependence of dispersion and nonlinear parameters on the fiber mode profile related by the equations (1.7) and (1.17) is the key to achieve their longitudinal variations by changing the cross-section. For the targeted pulse propagation, we have chosen a Bragg fiber cross-section where light is guided by photonic bandgap method. Properties of such fibers can be customized by suitably designing its transverse cross-section to realize the requirement. Moreover, its exclusive multilayered cladding structure eventually provides a somewhat bend-insensitive transmission of light compared to other PCFs. Since, the method of light guidance in Bragg fibers is different from standard step or graded index fibers, it is important to discuss the theory to solve for fiber modes, propagation constant, and confinement loss.

3.2.1 Theory of transfer matrix method

As depicted in figure 3.1, the cross-section of the Bragg fiber is radially symmetric with periodic arrangement of a bilayer, comprising of a high-index dielectric of thickness d_1 followed by a low-index dielectric of thickness d_2, surrounding the low-index core region of radius a. The modal analysis of such arbitrary refractive index profile can not be performed analytically, and requires a complete numerical approach. Transfer matrix method (TMM) is one of the straightforward method that involves only matrix multiplications without any complex plane iteration, and can be easily implemented in computer based programming. TMM readily solves for modes that are guided as well as leaky in nature and provides corresponding propagation constants with the absorption loss or leakage loss, as required.

Considering the translational symmetry along z direction, and rotational symmetry along

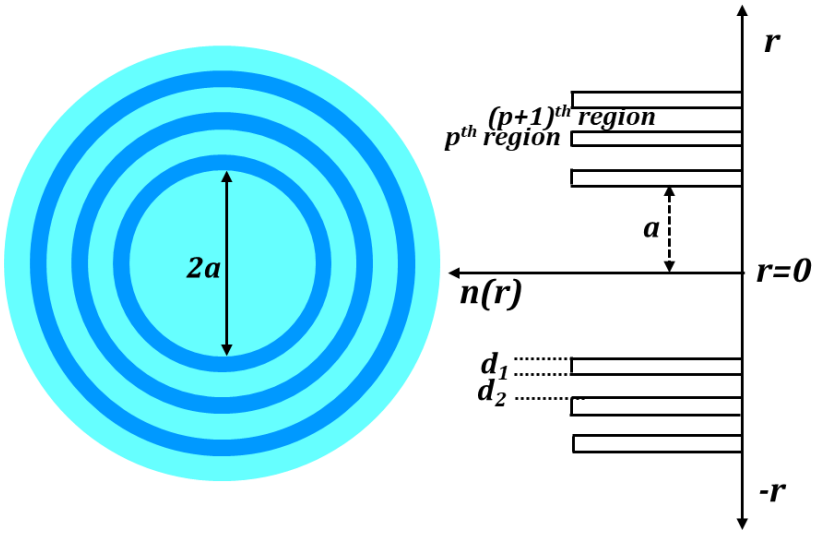

Figure 3.1: The schematic illustration of a standard Bragg fiber cross-section along with the radial variation of the refractive index.

ϕ direction, the modal field can be written in the separable form as,

$$\psi(r,\phi,z,t) = R(r)\exp[il\phi]\exp[i(\omega t - \beta z)], \tag{3.1}$$

where, β is the propagation constant, $l = 0, 1, 2, 3$ is the angular mode number, and $R(r)$ is the radial field part in the pth region of the fiber cross-section that must satisfy the following wave equation under scalar approximation,

$$r^2\frac{d^2R}{dr^2} + r\frac{dR}{dr} + [(k_0^2n_p^2 - \beta^2)r^2 - l^2]R(r) = 0, \tag{3.2}$$

where, k_0 is the free space wave number, n_p is the refractive index of pth region. For the solution of fundamental mode only, $l = 0$ and equation (3.2) becomes,

$$\frac{d^2R}{dr^2} + \frac{1}{r}\frac{dR}{dr} + [(k_0^2n_p^2 - \beta^2)]R(r) = 0. \tag{3.3}$$

Since, the confinement of the mode has to occur in the low-index region, the solution of equation (3.3) expressed as the family of Bessel function takes the form,

$$R(r) = A_pJ_0(\kappa_p r) + B_pN_0(\kappa_p r), \quad \text{for } \beta^2 < k_0^2n_p^2 \tag{3.4}$$

where, $\kappa_p^2 = k_0^2n_p^2 - \beta^2$. In scalar approximation, the boundary condition requires continuity of $R(r)$ and dR/dr at each interface. Thus, at pth layer they are expressed as [Morishita, 1981],

$$\begin{bmatrix} R \\ \frac{1}{\beta}\frac{dR}{dr} \end{bmatrix} = \begin{bmatrix} J_0(\kappa_p r) & N_0(\kappa_p r) \\ \frac{\kappa_p}{\beta}J_0'(\kappa_p r) & \frac{\kappa_p}{\beta}N_0'(\kappa_p r) \end{bmatrix} \begin{bmatrix} A_p \\ B_p \end{bmatrix} \tag{3.5}$$

Similarly, for $(p+1)$th layer, it takes the form,

$$\begin{bmatrix} R \\ \frac{1}{\beta}\frac{dR}{dr} \end{bmatrix} = \begin{bmatrix} J_0(\kappa_{p+1} r) & N_0(\kappa_{p+1} r) \\ \frac{\kappa_{p+1}}{\beta}J_0'(\kappa_{p+1} r) & \frac{\kappa_{p+1}}{\beta}N_0'(\kappa_{p+1} r) \end{bmatrix} \begin{bmatrix} A_{p+1} \\ B_{p+1} \end{bmatrix} \tag{3.6}$$

Solving equations (3.5) and (3.9) at $r = r_p$ to relate the unknown coefficients A_p, B_p, A_{p+1}, and B_{p+1}, one obtains,

$$\begin{bmatrix} A_{p+1} \\ B_{p+1} \end{bmatrix} = \begin{bmatrix} a_p & b_p \\ c_p & d_p \end{bmatrix} \begin{bmatrix} A_p \\ B_p \end{bmatrix} \qquad \text{where,} \tag{3.7}$$

$$\begin{bmatrix} a_p & b_p \\ c_p & d_p \end{bmatrix} = \begin{bmatrix} J_0(\kappa_{p+1} r_p) & N_0(\kappa_{p+1} r_p) \\ \frac{\kappa_{p+1}}{\beta} J_0'(\kappa_{p+1} r_p) & \frac{\kappa_{p+1}}{\beta} N_0'(\kappa_{p+1} r_p) \end{bmatrix}^{-1} \begin{bmatrix} J_0(\kappa_p r_p) & N_0(\kappa_p r_p) \\ \frac{\kappa_p}{\beta} J_0'(\kappa_p r_p) & \frac{\kappa_p}{\beta} N_0'(\kappa_p r_p) \end{bmatrix}. \tag{3.8}$$

Using the above prescription, the relation between the innermost layer (denoted by A_N and B_N) and the outermost layer (denoted by A_1, B_1) can be formed, and is given by,

$$\begin{bmatrix} A_N \\ B_N \end{bmatrix} = \begin{bmatrix} S_{11} & S_{12} \\ S_{21} & S_{22} \end{bmatrix} \begin{bmatrix} A_1 \\ B_1 \end{bmatrix} \tag{3.9}$$

where S_{ij}; $i, j = 1, 2$ are the matrix elements of the transfer function connecting all the intermediate layers. Since, the refractive index of the innermost layer (the core) is lesser than the outermost cladding layer, the fundamental mode becomes leaky for such fibers and calculation of the leakage loss becomes important. For $\beta < k_0 n_1$, the leaky mode solution requires it to be purely outgoing in the outermost region. This condition will be satisfied if one choose [Thyagarajan et al., 1991],

$$A_1 = iB_1. \tag{3.10}$$

Thus, from equation (3.9) the coefficients for innermost layers takes the form,

$$\begin{aligned} A_N &= A_1(S_{11} + iS_{12}), \\ B_N &= A_1(S_{21} + iS_{22}). \end{aligned} \tag{3.11}$$

Again, for $\beta < k_0 n_N$, the field is finite at $r = 0$, and it readily gives a complex eigenvalue equation,

$$B_N(\beta) = 0. \tag{3.12}$$

To solve for the propagation constant β from equation (3.12), one may consider a complex eigenvalue as a solution such that, $\beta_0 = \beta_{0r} - i\beta_{0i}$ and also may choose $B_N(\beta)$ to be of the form,

$$B_N(\beta) = B_N[\beta_0 + (\beta - \beta_0)] \approx B_N(\beta_0) + \frac{dB_N}{d\beta}\Big|_{\beta_0} (\beta - \beta_0). \tag{3.13}$$

Since, β_0 is complex, thus $B_N(\beta_0) = 0$, and

$$B_N(\beta) = \frac{dB_N}{d\beta}\Big|_{\beta_0} (\beta - \beta_{0r} + i\beta_{0i}). \tag{3.14}$$

From equtaion (3.14), one can estimate the function $|1/B_N(\beta)|^2$ and scanning this function over real β axis will readily provide a Lorentzian curve whose peak gives the real part of the propagation constant β and the full-width-at-half-maximum (w) provides the leakage loss (α) of the mode by the relation $\alpha = \pi w/\lambda$ in units of 1/m.

By implementing the aforementioned matrix method, the effective refractive index of the fundamental mode at any fiber cross-section can be estimated, and the dispersion parameter D and the GVD parameter β_2 can be readily obtained by using equation (1.11). Similarly, the mode effective area A_{eff} can be estimated from the knowledge of the mode profile, and thus the value of the nonlinear parameter γ is also possible to obtain by using equation (1.17).

3.2.2 Design of dispersion decreasing Bragg fiber

In this study, the cross-section of the fiber has been optimized to operate at 0.98 μm wavelength. The choice of the operating wavelength is based on the availability of the light sources at infrared wavelength range as well as on the possible lower absorption loss of the constituent glasses. The dielectric materials are chosen based on their transmission characteristic around the operating wavelength of the designed fiber. Specifications of two commercially available soft glasses have been chosen for a practical fiber design and simulation. The first step has been to optimize the thicknesses of the cladding bilayers at the operating wavelength. The thicknesses of the high and low index layers should be such that the operating wavelength lies within the bandgap. The optimization of the bilayer thickness has been an iterative process performed by solving the dispersion relation

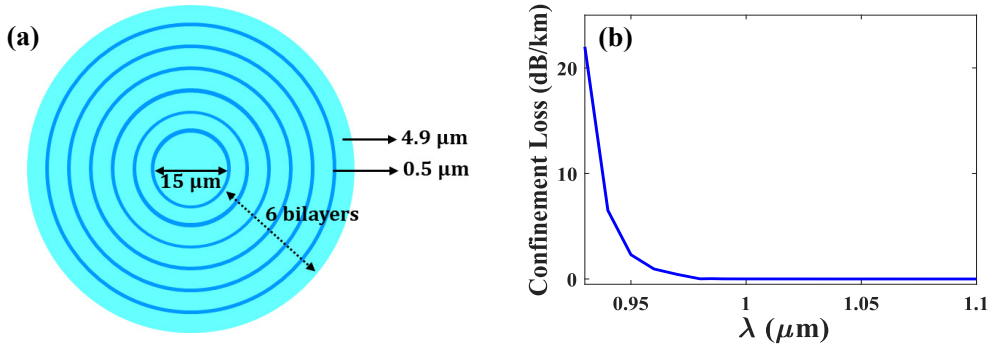

Figure 3.2: (a) The schematic of the designed Bragg fiber, (b) the variation of the confinement loss for the fundamental mode in the designed fiber .

given in equation (1.48) in a MATLAB® code built in-house. From the obtained bandgap plot i.e., the $\omega - k_y$ plot, for a particular set of bilayer thickness, the effective refractive index n_{eff} can be estimated for the fundamental mode at the operating wavelength. Using the estimated n_{eff} in equation (1.49), one may easily obtain the core radius for the fundamental mode. Moreover, the bilayer dimensions have been optimized iteratively using equation (1.50). Finally, the bilayer thickness and the core radius have been optimized at a point where n_{eff} do not vary significantly for the fundamental mode. Following the said procedure, the optimized input cross-section of the Bragg fiber is as follows: core radius $a = 7.5$ µm, high index cladding layer thickness $d_1 = 0.5$ µm, and low index cladding layer thickness $d_2 = 4.9$ µm. Moreover, six bilayers in the cladding have been considered for an optimum performance. The schematic of the cross-section of the designed Bragg fiber is depicted in figure 3.2(a). Moreover, the confinement loss curve for the fundamental mode has been depicted in figure 3.2(b). Notably, the confinement loss of the designed Bragg fiber has been shown up to 1.1 μm only, as beyond this wavelength the chosen glass materials exhibit higher absorption losses which results in a large total optical loss i.e., confinement and material loss together, that eventually limits the long distance pulse propagation. At 0.98 μm, the estimated value of the confinement loss is 0.015 dB/km. Moreover, the fiber design has been such that the confinement loss of the first higher order mode is much larger than that of the fundamental mode, and thus it would die out faster leaving only the fundamental mode confined to the core. It is to mention here that for Bragg type fibers where the modes are leaky, the number of modes supported by the fiber is quantified by a estimating the differential loss between various modes supported by the fiber. It is estimated as the difference between the leakage losses of any two modes at a particular wavelength. In general, it is assumed that a Bragg fiber operates as an effectively single-mode fiber when the differential loss between the fundamental mode and any other higher order modes is greater than or equal to 20 dB. For the designed DDBF, at 0.98 μm the loss of the first higher order mode has been $\sim$ 18 dB/km for which it is likely to operate as an effectively single-mode fiber.

With the aforementioned fiber cross-section, confinement loss α, dispersion parameter β_2, and nonlinear coefficient γ have been estimated for the fundamental mode through the modal analysis by implementing TMM in a MATLAB® based code. At the input cross-section, the estimated parameter values are as follows: D = -17×10^{-3} ps.m^{-1}.nm^{-1}, γ = 1.7×10-3 W^{-1}.m^{-1}. The longitudinal dispersion variation has been obtained by considering the hyperbolic dispersion profile as assumed in [Hirooka and Nakazawa, 2004] of the form,

$$D(z) = \frac{D(0)}{1 + \Gamma_0 z}, \tag{3.15}$$

$D(0)$ is the dispersion at the initial fiber cross-section $z = 0$, and Γ_0 has been assumed to have a standard value of gain coefficient 28×10^{-3} m^{-1} constant over the fiber length. The longitudinally tapered fiber profile has been depicted in figure 3.3(a). The corresponding decreasing dispersion profile has been computed numerically by using equation (3.15) and is shown in figure 3.3(b). For a Bragg type fiber, the decreasing dispersion profile could be achieved by down-tapering of the fiber. Such fiber tapering is now-a-days a common technical process and can be performed using state-of-the-art fabrication techniques with utmost accuracy. The tapering of the fiber means that there will be a fixed ratio of the initial cross-section to the final cross-section either greater than (up-tapering) or less than (down-tapering) unity and the intermediate variation is linear for the simplest case. It is to note that due to tapering the nonlinearity parameter γ has been found to have a negligible variation along the fiber length, and considered as nearly constant. Likewise, for the loss parameter α, only confinement losses of $\sim 10^{-4}$ dB/m for the fundamental mode have been incorporated.

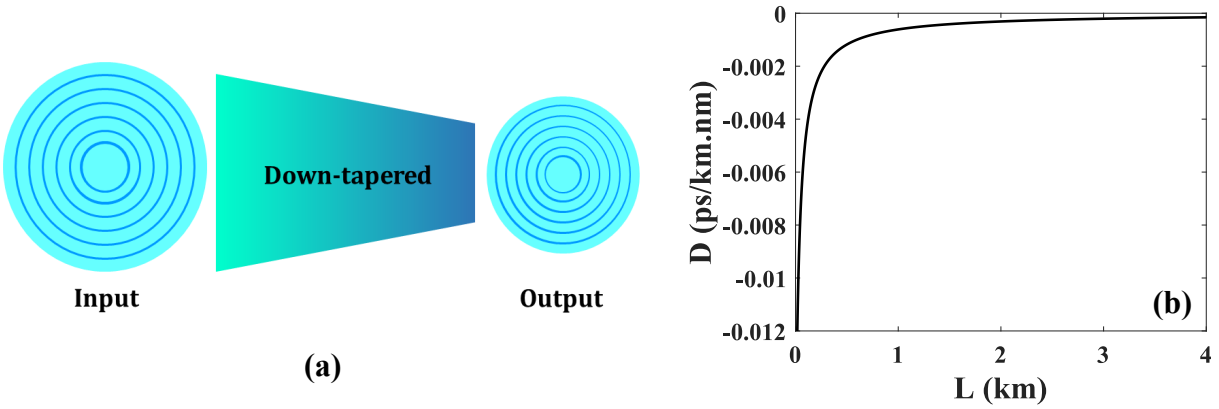

Figure 3.3: (a) the schematic representation of the longitudinally tapered fiber with input and output cross-sections, (b) the decreasing dispersion profile of the designed Bragg fiber.

3.2.3 Parabolic pulse formation in DDBF

In order to form parabolic pulses through a passive medium based DDBF, the fundamental requirement is to have a delicate balance between the longitudinally decreasing normal dispersion and the nonlinearity that essentially reshapes any standard input pulse shape into parabolic profile during its propagation through the DDF. As it has already been mentioned that in the designed DDBF, the second order dispersion parameter β_2 varies in such a way that the dispersion is longitudinally reducing. Hence, a particular form of NLS equation containing the dispersion decreasing term has been considered here. A slowly varying pulse envelope A(z, T) of a standard Gaussian pulse have been chosen as the input pulse form, and its evolution dynamics through the designed DDBF has been studied by numerically solving NLSE of the form,

$$\frac{\partial A}{\partial z} - i\frac{\alpha}{2}A + i\frac{\beta_2}{2}D(z)\frac{\partial^2 A}{\partial T^2} - i\gamma(\omega_0)|A|^2 A = 0, \tag{3.16}$$

where, β_2 and γ are the GVD and nonlinear parameters as estimated from modal analysis at the initial fiber cross-section, and $D(z)$ is an array containing dispersion values at various fiber length obtained by the equation (3.15). The NLSE has been solved numerically implementing SSFM in a MATLAB® code developed in-house.

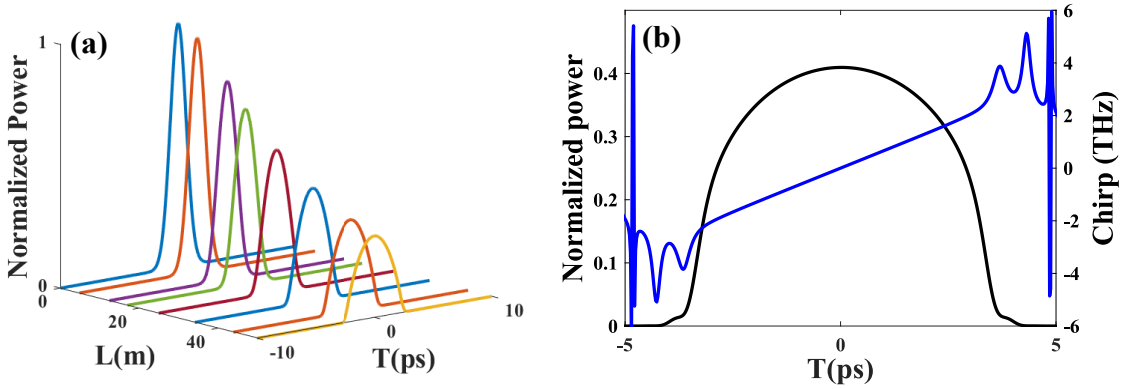

Figure 3.4: (a) The evolution of a Gaussian pulse as input into an output parabolic one through 50 m long designed DDBF, (b) the developed linear frequency chirp (blue curve) across the entire width of the parabolic pulse (black curve) at the end of 50 m.

The evolution of an unchirped Gaussian pulse of peak power 100 W and full-width-at-half-maximum (FWHM) 3.0 ps has been observed through the 50 m long designed DDBF. The evolution of the input pulse is depicted in figure 3.4(a). We can observe that gradually over the length of the fiber, the Gaussian profile is reshaped into a parabolic one. This is quite interesting to realize that in a dispersion varying landscape, the changing dispersion and nonlinearity accumulates the phase in such a way that it takes a parabolic form. Moreover, the essence of self-similar evolution lies in the fact that when the width is widening, the power profile is also being scaled in such a way that the entire parabolic shape is maintained. In figure 3.4(b), the variation of the frequency chirp developed during the propagation is shown. It can clearly be seen that the chirp is linear across the entire width of the formed parabolic pulse which holds the importance of such pulses being robust against strong nonlinearity. In the next section, the formation and stability of such parabolic pulse with a dark pulse in the background has been investigated through the DDBF.

3.3 Propagation of background guided parabolic pulses in DDBF

In this section, the evolution of background guided ultrashort pulses will be presented. Two standard and commercially available pulse forms, Gaussian and hyperbolic secant (sech), have been chosen as the input pulse. The dark pulse at the background of the input pulse has been chosen to be a hyperbolic tangent (tanh) pulse. It has earlier been mentioned that a tanh pulse can evolve self-similarly under a delicate balanced environment of dispersion, nonlinearity, and gain, and are widely known as dark similaritons [Kruglov et al., 2003]. Moreover, interactions between two and three such dark similaritons with a compact parabolic background have been reported in a dispersion managed fiber [Wu et al., 2009]. However, the evolution of a bright pulse guided by a dark pulse in an all-lossy environment has not been explored yet, and have been studied here through the designed DDBF to analyze the stability of the pulse combination over a single pulse form.

3.3.1 Evolution of tanh-guided Gaussian input pulse

The first set of investigation involves a Gaussian pulse guided by a tanh pulse to be propagated through the designed DDBF. The initial pulse specifications are as follows: the Gaussian and the tanh pulses have been chosen to have the identical peak power of 100 W; FWHM of the Gaussian input has been 3.0 ps, and for the tanh input has been 0.3 ps. Moreover, both the pulses are centered at 0.98 μm. The evolution of the pulse combination through the designed DDBF have been studied in-depth. The temporal profile of the input pulse (normalized) have been depicted in figure 3.5(a) where the peak power has been reduced than unity due to the presence of the tanh pulse at the center. One should note that if the power of the tanh background is reduced, then the depth of the dip will automatically be decreased by rising the peak values of the input pulse. The pulse combination has been allowed to propagate over several kilometers of the DDBF and the output pulse profiles and developed frequency chirps are observed at the end of 4 km. The temporal profile of the output pulse has been depicted in figure 3.5(b) in which a parabolic shape of the bright

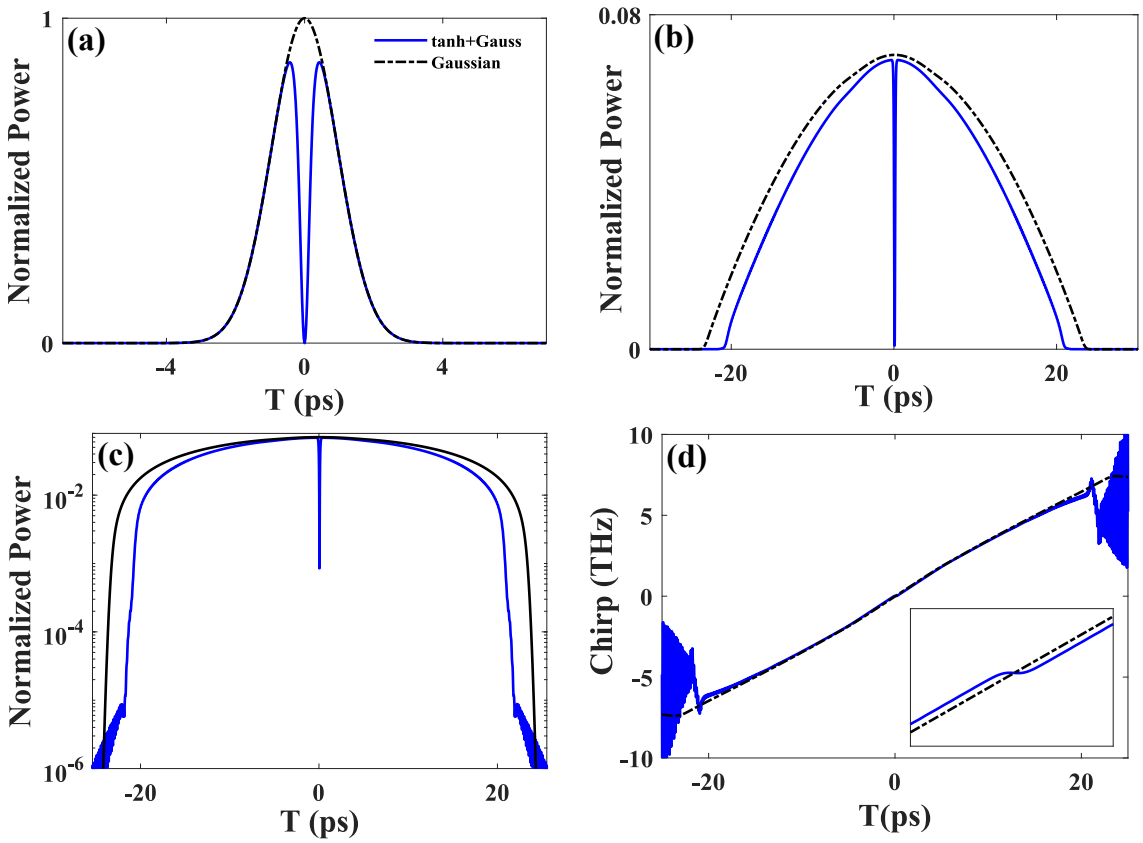

Figure 3.5: (a) The input pulse profiles, (b) the output pulse profiles, (c) the logarithmic plots of the output pulses, and (d) the output chirp variations of the tanh-guided Gaussian pulse (blue curve) and the single Gaussian pulse (black curve) through the 4 km long designed DDBF.

pulse can be explicitly observed along with the tanh pulse to be intact at the center. However, the normalized peak power has reduced as it has largely broadened in width (output FWHM $\sim$ 20 ps). Such large broadening is due to a large accumulation of dispersive phase mainly. It is to mention here that the presence of the tanh pulse in the background has an overall effect on the pulse peak power which is responsible for triggering strong nonlinear interactions. The reduction in the peak power eventually lowers the possibility of larger nonlinear phase accumulation compared to the dispersive one. Thus, it can be emphasized that this bright-dark pulse combination has essentially following a dispersion dominated pulse reshaping leading to a steady state regime. It is clear from the figure 3.5(b) that the output is smoother up to 4 km of the DDBF. Figure 3.5(c) shows the logarithmic plot of the output pulse profile where the top hat profile is the signature of the tempo-

ral parabolic shape at the output. The presence of the central dip is due to the tanh pulse which can be controlled by tuning the power and width of the guiding background. The evolution of the tanh-guided Gaussian pulse through the DDBF has been stable and smooth indicating its potential for long-distance propagation. Moreover, the developed frequency chirp for the pulse combination has been linear across the entire pulse width having a small kink corresponding to the central dip shown in figure 3.5(d). The monotonic chirp of the tanh-guided Gaussian pulse indicates that the combination could survive over several kilometers self-similarly through the DDBF.

3.3.2 Evolution of tanh-guided Hyperbolic secant input pulse

Here, the evolution of a hyperbolic secant pulse (sech) guided by the tanh pulse has been presented. As before, the input parameters for sech pulse and the tanh pulse have been chosen to be as follows: peak power = 100 W for both pulses, whereas FWHM for sech pulse has been 3.0 ps, and that for the tanh input has been 0.3 ps; both pulses are centered at 0.98 μm. Again the pulse combination has been allowed to evolve through several kilometers of the designed DDBF. The input temporal profile (normalized) has been depicted in figure 3.6(a), with a reduced peak power due to the presence of the dark pulse at the background. At the end of 4 km, the temporal

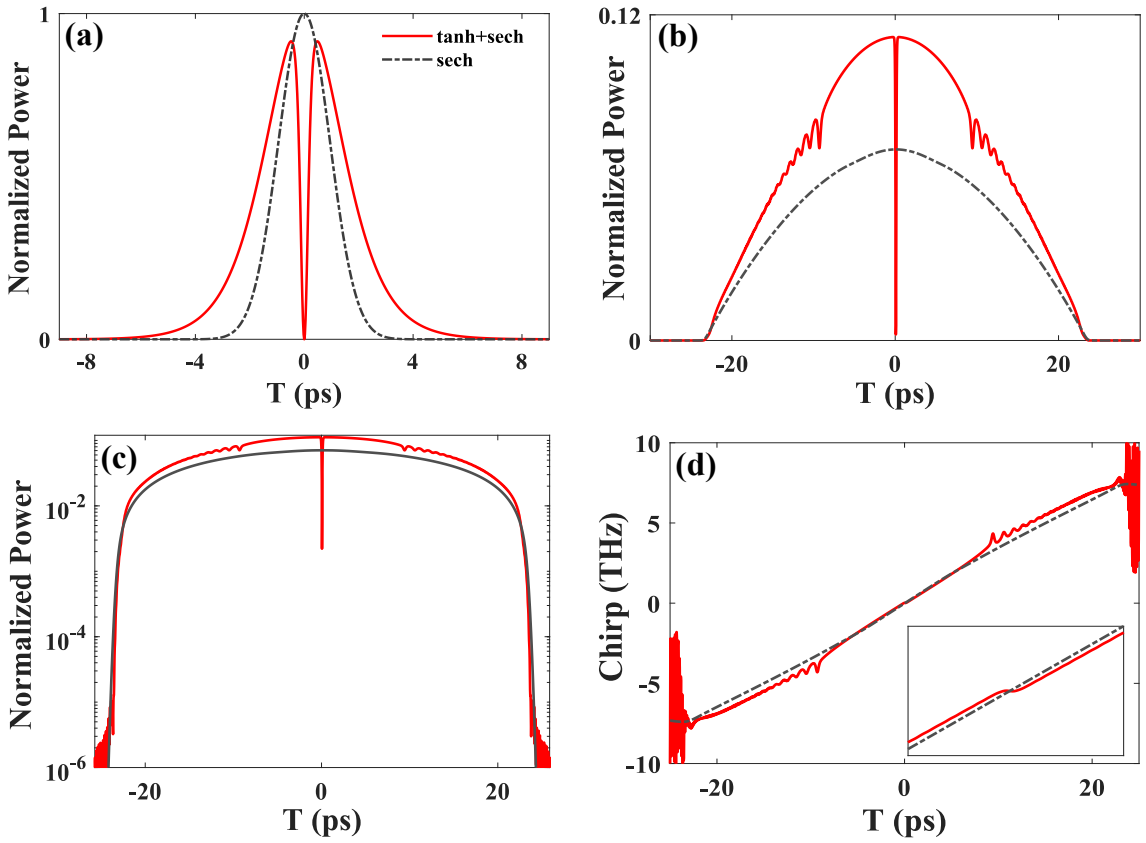

Figure 3.6: (a) The input pulse profiles, (b) the output pulse profiles, (c) the logarithmic plots of the output pulses, and (d) the output chirp variations of the tanh-guided sech pulse (red curve) and the single sech pulse (grey curve) through the 4 km long designed DDBF.

profile of the output pulse have been depicted in figure 3.6(b) in which a significant change can be observed in the output parabolic shape. Here also, the broadening of the pulse has been observed (output FWHM 20 ps) resulting mainly from the dispersion. One can explicitly observe difference in the stability of the self-similar evolution for the current pulse combination. It is clear from the figure 3.6(b) that there are some distortions in the output pulse profile which dictates that the pulse has entered the wave-breaking regime. Figure 3.6(c) is the logarithmic plots of the output

pulse profiles. The top hat profile is the signature of the temporal parabolic shape at the output with the central dip due to the presence of the tanh pulse. The tanh-guided sech input has evolved to a parabolic profile (characterized by the top hat log plot) but with certain oscillations/ripples at its edges which indicate a clear limitation of its maximum stable propagation length and its asymptotic evolution. This can be understood as the basic difference between the two pulse forms; from the expressions relating the pulse width T_0 to the pulse FWHM T_{FWHM} given as [Agrawal, 2019c],

$$T_{FWHM} \approx 1.665T_0, \qquad \text{and} \qquad T_{FWHM} \approx 1.763T_0 \tag{3.17}$$

for the Gaussian and the sech pulse, respectively indicate that the sech pulse with the identical FWHM as Gaussian will actually be a shorter pulse. Thus, the dispersion as well as the nonlinear effects have occurred faster for the latter combination leading to a propagation instability. Moreover, the developed frequency chirp for the pulse combination has a non-monotonic nature with a small kink at the center as shown in figure 3.6(d). One may observe small oscillations in the chirp profile at the same time-scale where ripples at temporal profile has occurred, which eventually reassures the onset of wave-breaking. Such non-monotonic nature of the chirp for tanh-guided sech pulse is a clear indication that over further propagation it will undergo complete wave-breaking.

3.3.3 A comparative study

For a better understanding of the effect of background guiding, we have compared the results obtained from the evolution of the background-guided pulses with the observations made from the propagation of a single Gaussian pulse and a single sech pulse of same power and FWHM through the designed DDBF. Figures 3.5(a) and 3.6(a) depict the single Gaussian and single sech inputs, each with peak power = 100 W and FWHM = 3.0 ps. They have been allowed to propagate through the DDBF over 4 km and the output pulse profiles (both linear and log plot) and the chirp variation for the Gaussian and the sech input have been depicted at the end of 4 km in figures 3.5(b) – (d), and in figures 3.6(b) - (d), respectively. The top hat profile in the logarithmic variation of the output pulses again indicate that the output is a parabolic pulse. Moreover, the chirp variations for both the evolution are also linear.

From the observations made so far, it is established that due to the presence of the tanh pulse at the background of both the Gaussian and sech pulses, the pulse reshaping through the DDBF has not deteriorated much and it has evolved smoothly with the main seed pulse without any further significant evolution of its own. Now to understand the impact of its presence on propagation, the evolution of the misfit parameter M as a function of fiber length L has been plotted for all four types of input pulses – the two bright-dark pulse combinations, and the two single bright pulses. The misfit parameter between the pulse temporal intensity profile $|A|^2$ and the parabolic fit $|p|^2$ of the same energy is defined as,

$$M^2 = \frac{\int [|A|^2 - |p|^2]^2 dT}{\int |A|^4 dT}, \tag{3.18}$$

where the expression for the parabolic fit with peak power P_p and pulse duration T_p is given by:

$$p(T) = \begin{cases} P_p(1 - \frac{T^2}{T_p^2}) & \text{for} \quad |T| \leq |T_p| \\ 0 & \text{for} \quad |T| > |T_p| \end{cases} \tag{3.19}$$

A gradually decreasing value of M indicates the better fit to the targeted parabolic waveform. We have considered $M < 0.04$ to be sufficient for a pulse to be parabolic. From figure 3.7(a) it is clear that the reshaping of single Gaussian to parabolic is faster than the tanh guided Gaussian

and also it has reached a minimum of 10^{-4} around 2.5 km of the total fiber length. However, it has started to rise again with further propagation. The increment in the misfit parameter implies the gradual change in the pulse shape away from the parabolic form indicating that the formed parabolic pulses has been the intermediate transient state of propagation. This feature has been

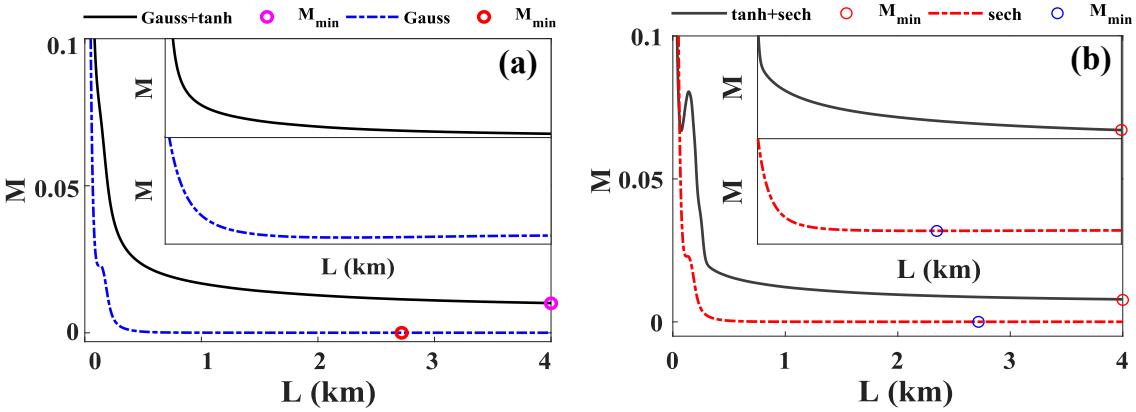

Figure 3.7: The variation of misfit parameter M along the length of the DDBF for (a) tanh-guided Gaussian and a single Gaussian pulse, (b) tanh-guided sech and a single sech pulse.

explicitly shown as inset of figure 3.7(a). On the other hand, the tanh guided pulse slowly evolves into the parabolic one with a minimum misfit value of 10^{-3} at around 4 km i.e., at the fiber end. Also, on further propagation it has kept on decreasing, clearly indicating the asymptotic nature of pulse evolution (inset of figure 3.7(a)). Similarly, figure 3.7(b) depicts the faster evolution of the single sech pulse into parabolic than that for the pulse combination. An initial distortion near 100 m fiber length can be observed for the tanh guided sech pulse, however it gradually has reshaped into the parabolic profile with further propagation. In this case also, we have obtained an asymptotic nature of evolution for tanh+sech pulse with a gradual fall down of M (shown as inset of figure 3.7(b)) whereas single sech pulse starts rising up after certain length of the DDBF. Thus, the presence of tanh pulse at the background actually stabilizing the pulse propagation and gives a robust parabolic pulse with linear chirp at the end of a passive fiber. It has earlier been mentioned that the parabolic pulse formation depends on the input energy content rather than pulse amplitude or width. Here also, one can observe that the dark pulse at the background of the bright pulse redistribute the energy in such a way that it has readily entered the steady state regime of propagation and the asymptotic evolution has stabilized the pulse. However, comparison between the two pulse combinations reveals that the evolution of tanh-guided Gaussian pulse is more stable than the tanh-guided sech one, which is also input pulse specification dependent. A stable propagation of sech+tanh pulse combination over such long distance may be achieved with the proper choice of input pulse parameters.

Moreover, the output spectral profiles of the four pulse types have been depicted in figures 3.8(a) and 3.8(b). The output spectra of the single Gaussian and the single sech pulse have exhibited a smooth flat top with a sharp intensity dip at the center, whereas the tanh guided respective pulse combinations have shown oscillations/ripples at their output along with the central intensity dip. Moreover, the ripples in the spectrum of tanh+sech pulse combination have observed to be much random compared to that obtained from the tanh+Gaussian pulse form. It is to mention here that the small oscillations have found to be within the 10dB bandwidth of the spectrum showing a nearly comb-like intensity profile for both pulse combinations as shown in figures 3.8(c), and (d), respectively. A closer look of the spectra reveal that the output spectra of the tanh+Gaussian pulse has more prominent oscillatory features compared to that obtained from tanh+sech combination. On further tuning of such nearly comb-like profile of the background guided pulses, it may be useful for applications like comb-spectroscopy.

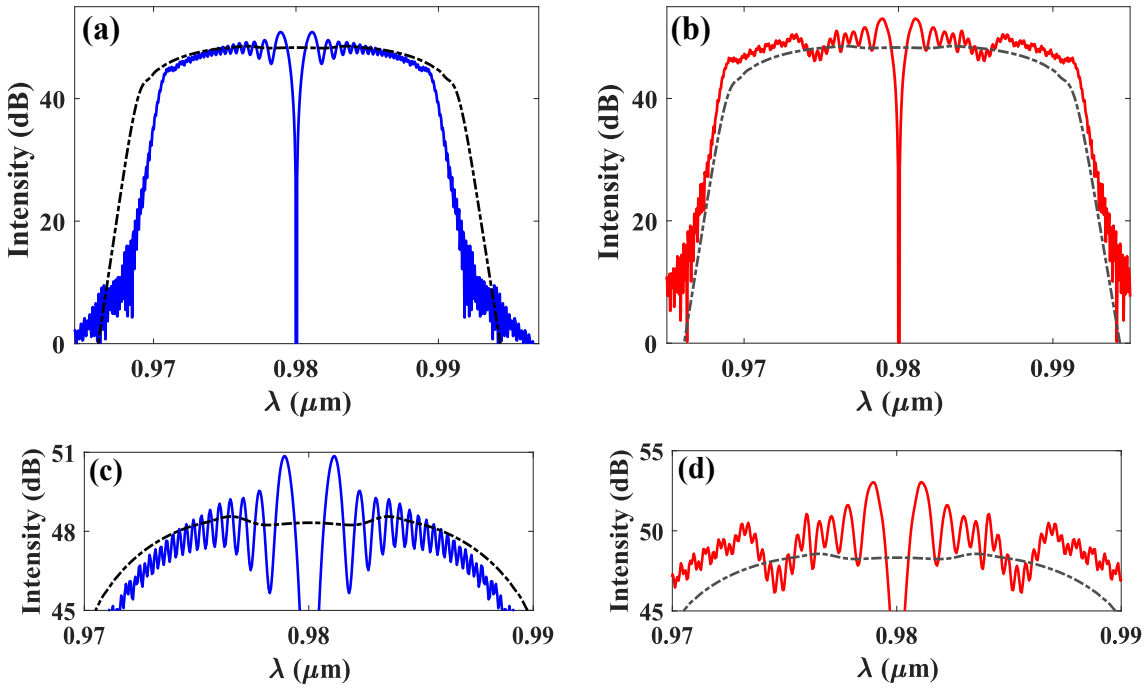

Figure 3.8: The output spectra of (a) tanh-guided Gaussian and single Gaussian pulse, (b) tanh-guided sech and single sech pulse at the end of the 4 km long DDBF; (c) and (d) shows the closer look at the top of the respective spectral profiles.

3.4 Conclusions

In summary, a stable self-similar evolution of background-guided parabolic pulses over kilometer long distance through an all-solid dispersion decreasing bandgap fiber has been demonstrated in this chapter. Unlike gain-assisted fibers, the self-similar/asymptotic evolution of the formed parabolic pulses through passive fibers are often challenged by the fiber loss and dispersion, leading to an intermediate transient pulse state. In order to retain the self-similar behavior of the evolved pulse over long distances, an input pulse customization technique has been implemented, in which a dark optical pulse, widely known as tanh pulse, has been put at the background of certain bright pulses of Gaussian and sech forms. The aim has been to control the total energy of the combined input pulse which will gradually turn on the reshaping process by suitably counterbalancing the accumulation of linear and nonlinear phases to sustain over longer distances. To realize the concept, a standard Bragg fiber with longitudinally decreasing dispersion profile has been designed to be operated at 0.98 μm, and the combination of the bright and the dark pulse has been allowed to propagate through the designed fiber. At the end of 4 km of the designed DDBF, an asymptotically evolved parabolic pulse with an intensity dip at the center has been observed. It has been observed that the presence of the tanh pulse at the center has redistributed the energy of the initial pulse which eventually have lowered the possibility of strong nonlinear interactions for both the pulse combinations. Thus, pulse evolution has been mainly dispersion dominated with balanced nonlinear effect required for pulse reshaping. For a qualitative comparison, a single Gaussian pulse and a single sech pulse of same input parameter have been allowed to propagate through the same DDBF which have shown an intermediate transient state of evolution leading to OWB, thereby inferring the pulse customization technique as a better technical approach for stable long distance light delivery.

3.4.1 Applications

From application point of view, such background guided pulse propagation is of immense importance for long distance distortion-free light delivery. From the results of misfit parameter evolution, it can be concluded that a tanh guided Gaussian pulse would carry more energy over longer distances than its single Gaussian counterpart without triggering significant nonlinear effect. The striking result of this investigation is that the evolution of pulses nearly asymptotic in a passive fiber that matches the evolution of parabolic pulses in amplifiers mitigating the issues related to amplifier-based parabolic pulse formation. Moreover, its self-similar nature of propagation is maintained, thus resulting in no or little further temporal distortion which makes it suitable for long distance delivery. For high energy applications like precision machining [Bračun and Selak, 2018], bio-medical imaging [Lee et al., 2013], laser-launched detonation processes [Weise et al., 2004; Curtis et al., 2014; Gottfried, 2018; Wang et al., 2022] where very high energy ($\sim$ several mJ) optical pulses have to be delivered over distances from several meters to few kilometers, such background guided pulse will undoubtedly meet the requirement for its robust nature. Furthermore, the nearly comb-like output spectrum corresponding to the tanh guided pulse is also very interesting upon in-depth study for a potential application in all-fiber based comb spectroscopy [Nakajima et al., 2018].

3.4.2 Impact statement

The requirement of passive medium based formation of parabolic pulses stems from the technical challenges such as limited amplifier bandwidth, and noises which are inevitable for pulse reshaping in gain-assisted fibers. In this chapter, it has been aimed to provide a solution to the issue related to the asymptotic evolution of parabolic pulses in passive medium based fibers eliminating the intermediate transient state of propagation which readily distorts the parabolic form. To counter this challenge, an input pulse customization approach has been adapted in which a dark optical pulse has been used in the background of a bright pulse to redistribute the combined pulse energy which results in an overall dispersion-dominated pulse reshaping. The outcomes of this chapter should directly impact the future endeavors in the area of optical pulse reshaping. Particularly, the dynamics of the dark pulses, and the effect of their presence during the evolution of the bright pulse may bring out certain exclusive features providing robust solutions compared to the existing techniques not only for fiber based pulse reshaping but also for other waveguide platforms. Precisely, this pulse-customization technique will be much suitable for application areas that can allow a minimum modification keeping the major part of the system intact to realize the desired outcome.